

An intermediate complexity AGCM simulations of climate response to a doubling of atmospheric carbon dioxide

Irena Nimac¹ and Ivana Herceg-Bulić²

¹ Meteorological and Hydrological Service of Croatia, Zagreb, Croatia

² Department of Geophysics, Faculty of Science, University of Zagreb, Zagreb, Croatia

Received 2 May 2016, in final form 26 April 2017

Atmospheric response to doubled carbon dioxide concentration is estimated by analyzing 35-member ensemble mean made by an atmospheric general circulation model of intermediate complexity. Simulated changes in the mean fields are evaluated for winter (January-February-March) and summer (July-August-September) seasons. Results show that doubled CO₂ concentration causes warming of around 2 °C at all levels in the model. At the surface, the largest temperature change is found over the polar areas; while at the higher levels considerable warming is found mostly over the continental parts. Atmospheric warming at the 300 hPa level is accompanied by cooling over the polar areas. At the levels above 300 hPa, temperature drops globally. Changes in jet stream occur at Northern Hemisphere with larger winter amplitudes. During the respective winter, stratiform precipitation significantly increases at the higher latitudes of both hemispheres and decreases mostly over the oceans. Over the Northern Hemisphere, convective precipitation is significantly increased during the summer. Over the southern part of tropical Pacific, stratiform and convective precipitation is decreased during the both seasons. Results also demonstrate that indirect impact of increased CO₂ concentration (*i.e.* effects associated with changes in the lower boundary conditions) generally has a stronger contribution to the tropospheric warming than direct CO₂ impact (*i.e.* the impact associated with absorption and emission of longwave radiation).

Keywords: climate change, doubled carbon dioxide concentration, intermediate complexity model, direct CO₂ effect, indirect CO₂ effect

1. Introduction

Throughout the past few decades, interest for climate change associated with elevated concentration of greenhouse gases, has substantially increased due to numerous consequential effects on human health, ecosystems, agriculture, water sources, etc. The climate change is discernible everywhere, from the tropical to

polar areas, over the oceans, small islands and large continental parts. Variations in climate can be caused by natural (*e.g.* sea-atmosphere interactions, volcanic eruptions, changes in solar radiation) and anthropogenic (human-induced) processes. Anthropogenic influence significantly contributes to the global warming and it has increased considerably as a consequence of industrial growth. Urbanization, burning of fossil fuels, deforestation and other soil change processes increase greenhouse gases (GHGs) concentrations in the atmosphere. GHGs absorb long-wave radiation from the ground and radiate it in all directions, and the component directed back to the Earth's surface causes additional warming of the lower atmosphere. A number of gases are involved in enhancement of greenhouse effect, like water vapour, carbon dioxide, methane, nitrous oxide, chlorofluorocarbons and tropospheric ozone. Water vapour is strong and the most abundant GHG, but its atmospheric residence time is quite short (around 9 days), while some other GHGs could remain in the atmosphere for longer time and thus may contribute to the global warming more efficiently. The long-lived GHGs not only sustain global warming, but also drive positive water vapour feedback. Human impact on the climate is evident and extensively investigated (IPCC, 2014). There are a fullness of scientific evidence for anthropogenic contribution to the global warming what is based on observations, theoretical understanding of physical processes and state-of-art climate models.

According to the Fifth Assessment Report (AR5) of the Intergovernmental Panel on Climate Change (IPCC, 2014), warming of the climate system is unequivocal. There is observational evidence showing that each of the last three decades was successively warmer than any preceding decade since 1850, carbon dioxide concentrations have increased by 40% since pre-industrial times, primarily from fossil fuel emissions but also from net land use change emissions, Greenland and Antarctic ice sheets have been losing mass, glaciers continue to shrink, Arctic sea ice and Northern Hemisphere spring snow cover continue to decrease in extent. It is also reported that dominant cause of ocean warming is increase in energy stored in the climate system with more than 90% of energy accumulated during 1971-2010 period. The role of oceans in global warming was subject of many studies (Washington and Meehl, 1989; Manabe et al., 1990; Manabe et al., 1991). Oceans play a significant role in warming since SST increase induces sea-ice melting which consecutively causes further temperature increase (positive feedback). Also, ocean dynamics help to ameliorate the increase of SSTs (Henderson-Sellers, 1987) and oceans substantially contribute to the continental warming (*e.g.* Hoerling et al., 2008; Compo and Sardeshmukh, 2009; Dommenges, 2009).

The need of investigations related to the climate change and associated physical processes is undoubted, particularly because there is an abundance of possible effects and consequences of climate change, and some of them could be irreversible (Solomon et al., 2009). Climate models are useful for such investigations

with a purpose to project climate conditions into the future. There is a hierarchy of models of different complexity that may be used (Kucharski et al., 2013). Among them, intermediate complexity models have been found as very convenient. Due to their computational efficiency, they are suitable for creating of various targeted and idealized numerical simulations enabling a deeper insight into the problem of climate change and associated physical processes.

Increased CO₂ concentration affects the climate system in two ways, directly and indirectly. Direct impact manifests as an additional warming due to absorption and radiation processes in the atmosphere. Main additional effects from changes in CO₂ absorption are strong stratospheric cooling, moderate increase of land-surface temperatures and a positive Arctic Oscillation response (Bracco et al., 2004; Shindell et al., 1999). Indirect impact of increased CO₂ is realised through the processes induced by changes in lower boundary conditions which are caused by elevated CO₂ (like modification of SSTs, soil temperature, albedo, etc.). Modelling approach enables separation of different contributors and distinguishing of their impacts. Thus, some existing results indicate that the atmospheric response to indirect forcing is stronger than that to the direct forcing (*e.g.* Stephenson and Held, 1993)

In this paper, idealized simulations of climate change associated with doubled CO₂ are made by AGCM of intermediate complexity and they are also used to explore direct and indirect CO₂ influence. The same model and similar simulations were used to assess the change of ENSO teleconnections in a warmer climate (Herceg-Bulić et al., 2012). The study is organized as follows. In Sect. 2, the model and experimental design are described. Changes in temperature, zonal wind and precipitation at selected layers are shown in Sect. 3. At last, Sect. 4 provides conclusions and discussions of main points of the study.

2. Numerical simulations

2.1. Model description

Model used for this study is ICTP AGCM (International Centre for Theoretical Physics Atmospheric Global Circulation Model). The model is of intermediate complexity with eight vertical levels and triangular truncation of horizontal spectral fields at total wave number 30 (T30L8). An earlier model version with five vertical levels is described in details with its climatology and variability in Molteni (2003). ICTP AGCM is hydrostatic, σ -coordinate model based on a spectral dynamical core developed at the GFDL (Held and Suarez, 1994). It uses relatively simplified physical parameterizations and spectral transform in the vorticity-divergence form (Bourke, 1974) with semi-implicit treatment of gravity waves. The parameterized processes include short- and long-wave radiation, large scale condensation, convection, surface fluxes of momentum, heat and

moisture and vertical diffusion. Land and ice temperature anomalies are determined by simple one-level thermodynamic model and inclusion of those in ICTP AGCM amplifies seasonal cycle of temperature (Herceg-Bulić and Branković, 2006). Using the first model version of ICTP AGCM with five vertical levels, Molteni (2003) showed that the model simulates atmospheric flow realistically, especially during the boreal winter. Next model version with seven vertical levels has been considerably improved compared to the previous version. The comparison of the improved model version results with NCEP/NCAR reanalysis (Kalnay et al., 1996) for period 1952–2001 confirms that ICTP AGCM successfully simulates the forced and internal components of the atmospheric interdecadal variability.

In this study, we are using the model version with eight vertical levels with horizontal spectral truncations T30 (about 3.75×3.75 degrees horizontal resolution). A more detailed description of the model can be found in Kucharski et al. (2013). Computational efficiency of ICTP AGCM and its results covering broad range of climate variability (Kucharski et al., 2013, and references therein) justify using this model for examining the changes of general atmospheric circulation associated with increased CO₂ concentration.

2.2. Experimental design

The results from four ICTP AGCM experiments are analysed in the paper:

(a) CTRL experiment: ICTP AGCM is forced with observed SSTs at the lower boundary and average CO₂ concentration for the period 1961–1990. SSTs are given as monthly averages from a long time series of NOAA_ERSST_V2 data (Smith and Reynolds, 2004) and are blended with sea-ice monthly climatology values from the Hadley Centre (Rayner et al., 2003). For sea-ice and upper soil level the blending is based on estimation of temperature fluctuations via so-called extended force-restore method (Hirota et al., 2002). It takes into account the net heat flux into the ground (sea-ice), prescribed climatological temperatures and their seasonal cycle.

(b) 2xCO₂ experiment: ICTP AGCM is forced with climatological SST and sea-ice fields that correspond to the doubled CO₂ concentration. Monthly varying SST anomalies (*i.e.* their interannual variability) are kept the same as in CTRL experiment. SST and sea-ice climatology are provided by Hadley Centre AOGCM model integration (HadCM3) forced with doubled CO₂ concentration. HadCM3 is fully-coupled model that includes atmosphere (Gordon et al., 2000) and ocean (Pope et al., 2000) components and is often used in climate change simulations (IPCC, 2007). HadCM3 run is performed with increasing CO₂ concentration by 1% per year for 70 years until concentration is doubled, and then integrated for the next 150 years with constant CO₂ (similarly as in the analyses of doubling

CO₂ effects by Meehl et al., 2006; Merryfield, 2006; Turner et al., 2007; Hannachi and Turner, 2008). Recent changes of the sea-ice content are realistically represented by HadCM3 model, and model simulations indicate a reduction of Arctic sea ice content in the future as a consequence of anthropogenic impacts (Gregory et al., 2002).

(c) Indirect experiment (IND): indirect CO₂ effect is attained by employing the SST and sea-ice climatological fields corresponding to the HadCM3 AOGCM simulations with doubled CO₂, but the coefficient of absorption in the CO₂ band of the ICTP AGCM long-wave radiation parameterisation scheme is kept at the same value as in the CTRL run (*i.e.* it corresponds to 1xCO₂ concentration)

(d) Direct experiment (DIR): the coefficient of absorption in the CO₂ band of the ICTP AGCM long-wave radiation parameterisation scheme corresponds to the doubled CO₂ concentration with no changes in sea-ice and SSTs (*i.e.* sea-ice and SSTs are the same as in CTRL experiment). Doubled absorption leads to additional radiative forcing in ICTP AGCM model of around 4 Wm⁻² which is in good agreement with values from IPCC models (2007).

For each of four experiments, 35-member ensemble mean of 149-year long ICTP AGCM integrations were created. Every ensemble member of the same experiment is simulated with identical boundary conditions but with slightly different initial conditions. Initial conditions of simulations are different in a way of duration of initial diabatic warming in four model points in the tropical area. The first year of integration is discarded and the analysis provided in the paper refers to the total of 148 years. Because of relatively large size of ensembles and long integrations, we may consider results as statistically reliable.

2.3. Changes in the boundary conditions

Increased green-house gasses induces global warming which is also reflected as modified conditions at the lower boundary. Of particular interest for this study are changes in SST and sea-ice content and their impact on climate. Therefore, first we show January-February-March (JFM) and July-August-September (JAS) climatological fields for SST and sea-ice fraction that are used in 2xCO₂ and CTRL experiments as boundary conditions (Fig. 1.)

In general, surface of the world oceans is warmed in both seasons. The largest local warming is obtained in the north Pacific reaching the value of 3°C in JFM (Fig. 1a) and 5°C in JAS season (Fig. 1b). According to Meehl and Washington (1996), SST increase in the tropical Pacific that is observed during last decades may be connected with increased CO₂ concentration in the atmosphere. Relatively cool water appears in subtropical south Pacific (around 135°W), and that decrease of SST associated with equatorial warming has a direct effect on the local Hadley circulation and characteristic of precipitation

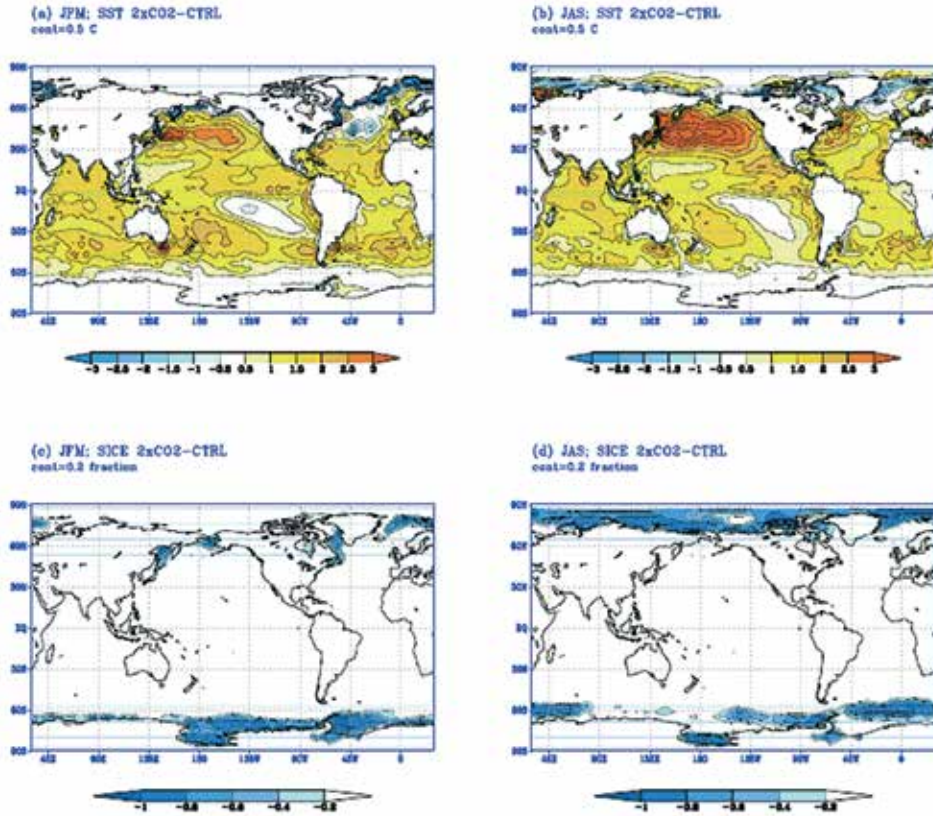


Figure 1. Differences between 2xCO₂ and CTRL for (a) SST in JFM; (b) SST in JAS; (c) sea-ice extent in JFM; (d) sea-ice extent in JAS. Contours every 0.7 °C in (a) and (b) and 0.05, 0.1, 0.3, 0.5, 0.7, 0.9 in (c) and (d).

(Herceg-Bulić et al., 2012). SST decrease that appears south of Greenland is related to the effects of deep overturning in the ocean model (Manabe et al., 1991), while negative SST anomalies in the northern polar region reflect the impact of sea-ice melting that cools the sea surface. In the equatorial Pacific and along the coast of South America, SST increase reaches values between 1.5 and 2°C.

Sea-ice reacts to both air and sea warming. The CO₂ concentration increase is accompanied with significant disappearance of sea-ice, especially pronounced in high latitudes during hemispheric summers. As sea-ice has a strong influence on heat balance over the oceans, changes in its extent and thickness are equally important as changes in SST (Jin et al., 1994). The reduction of sea-ice is involved in positive feedback process with ocean's surface warming. Namely, sea-ice melting reduces surface albedo and consequently increases absorption of solar energy maintaining further warming of the sea.

3. Results

Seasonal means are calculated as time mean of three successive months over the period 1961-1990 for winter (January-February-March) and summer (July-August-September) seasons. Spatial fields of seasonal means are presented here for each experiment at four vertical levels: surface, 925 hPa, 500 hPa and 300 hPa. Changes in the mean state are provided as a difference between the mean fields of experiments (2xCO₂ minus CTRL). Average temperature at each level is calculated as a spatial mean of temperature over Earth's surface to obtain global value and is also considered separately for each of the hemispheres. Statistical significance is estimated applying two-sided t-test for difference of the means (Wilks, 2006) at 99% level of confidence.

3.1. Impact on temperature

3.1.1. Surface and higher level temperature changes

Wintertime (JFM) temperature difference between 2xCO₂ and CTRL experiment at selected levels is shown in Fig. 2. There is relative warming of 2 °C at all levels with the greatest surface temperature change over the polar regions (Fig. 2a). The maximal local temperature increase with a value around 14 °C occurs in

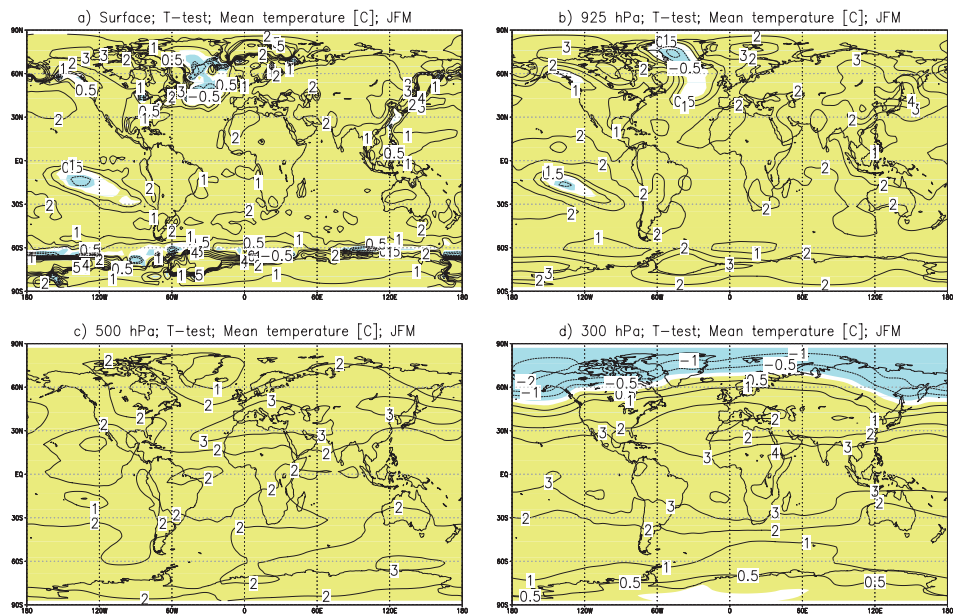


Figure 2. Temperature changes between 2xCO₂ and CTRL experiments for JFM season at: (a) surface; (b) 925 hPa; (c) 500 hPa; (d) 300 hPa. Shaded areas are significant changes with positive changes marked as full lines and negative changes represented as dashed lines. Contours: 0.5, 1, 2, 3, 4, 5, 14 °C.

the northern polar area, while along the coast of eastern Asia, coast of east Canada and over Alaska, the warming is around 5 °C. This positive temperature change is associated with sea-ice loss in those areas and indicates that region as a particularly sensitive to elevated green-house gases. Relative increase for around 2 °C affects broader parts of Asia and northeast Canada.

In comparison with temperature response at the surface, temperature changes at 925 hPa level are more uniform and mainly positive with slightly weaker amplitude. Local maximums coincide with those at the surface (Fig. 2b). Average warming of around 2 °C occurs over Antarctic, central and southern Europe, Asia, Australia, northern Canada and northwest Africa. Over the oceans, significant temperature increase is found over the northern part of Indian Ocean and northern equatorial Pacific. Negative temperature changes over Greenland and equatorial Pacific keep through the larger part of troposphere (not shown). Similar fields to that at 925 hPa remain until 500 hPa where local cooling disappear (Fig. 2c). At 300 hPa (Fig. 2d), distribution of JFM temperature changes shows zonal pattern. In tropical area temperature increase is 2 °C with few local maximums of around 4 °C. Temperature of the most northern parts is decreased, while around 60° N there is a belt with negligible temperature changes.

Summertime (JAS) temperature differences between 2xCO₂ and CTRL experiments at selected levels are shown in Fig. 3. Average warming of around 2 °C is simulated at all levels in the atmosphere. The strongest impact of doubled CO₂ is found again at the surface in polar region of the winter hemisphere (*i.e.* Southern Hemisphere) reflecting the impact of changes in sea-ice and SSTs

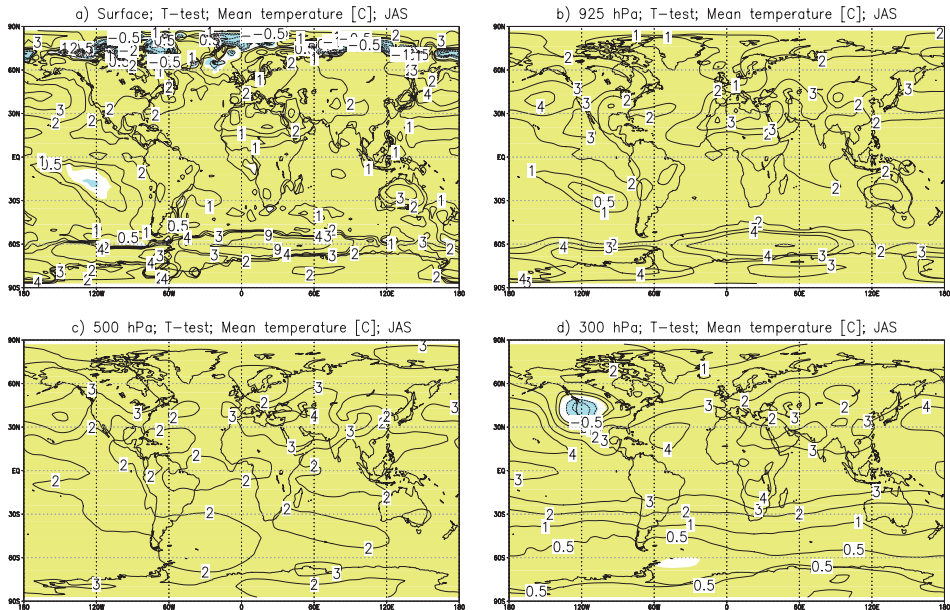


Figure 3. Same as Fig.2, but for JAS season. Contours: 0.5, 1, 2, 3, 4, 9, 16 °C.

(Fig. 3a). The largest temperature increase reaching 16 °C is found over Antarctica and coincides with significant sea-ice reduction there (Fig. 1d). However, temperature is declined over the northern polar region (due to sea-ice melting that cools the sea water and overlaying air). Local warming over the northern Pacific reaches 4 °C, while over the land there is a temperature increase of approximately 3 °C occurring over northern Africa, southwest Asia, northern part of North America and Australia. The influence of surface conditions is weakened at higher atmospheric levels, therefore temperature change achieves smaller amplitude there (Fig. 3b). In the upper atmosphere, the strongest warming remains over the north Pacific and Antarctica with another local maximum placed over the northern part of Arabian Peninsula. The effect of sea-ice melting and associated cooling of overlaying air in the Arctic region diminishes with height and at 925 hPa there is a warming of around 1 °C.

Continental parts of mid-latitudes are warmed with an average temperature increase of around 2 °C and areas with the greatest increase are North America, northern Africa, southern Europe, Arabian Peninsula, Russia and Australia. At higher atmospheric levels, local temperature maximums are weaker with relative warming around 2 °C spreading over the larger part of land (not shown). Similar temperature change distribution remains up to 300 hPa level where temperature change has almost zonal distribution (Fig. 3d). Temperature increase in the tropical region is around 3 °C and reaches 4 °C over the northern subtropical oceans. Negative temperature changes occur over the west America at 120° W, but they are not statistically significant. Negligible temperature changes are also simulated around 60° S.

According to the presented results, it is notable that simulated global warming is seasonally and regionally dependant. During the winter, polar regions are relatively warmer in comparison with the control winter climate, primarily due to sea-ice loss, while on the other hand, sea-ice melting during the summer reduces air warming over the sea (or even may cause cooling). At the higher atmospheric levels, the influence of sea-ice vanishes, and at 925 hPa and upper levels, the warming is simulated over the whole globe. Temperature change at 300 hPa has almost zonal distribution. Over the polar region of both hemispheres, there is relatively small positive temperature change during the respective summer, while cooling of the upper polar atmosphere is obtained during the respective winter. At the top two layers in ICTP AGCM (100 and 30 hPa), global stratospheric cooling is simulated (not shown) what is in accordance with the theory of stratospheric cooling due to climate changes (Thompson et al., 2012). The given changes are relatively consistent to those obtained by complex AOGCM projections for different climate scenarios in IPCC AR4 (Meehl et al., 2007) as well as with equilibrium changes in temperature means due to doubling CO₂ as reported in IPCC (2007).

Changes between 2xCO₂ and CTRL experiment are significant in both seasons at all selected levels.

3.1.2. Vertical structure of hemispheric and global temperature change

Average temperature at each vertical level is calculated by averaging seasonal temperature means over the Earth's surface, and separately for Northern and Southern Hemisphere. Global warming is obtained at all levels and for both seasons. At the surface level, global temperature increase is larger for the summer hemisphere with maximum at the 500 hPa (2.2 °C and 2.3 °C for JFM and JAS season, respectively). Simulated temperature changes at all selected levels are larger in JAS than in JFM season, even for both hemispheres. Generally, Northern Hemisphere exhibits stronger warming than its southern counterpart (at all levels except at 300 hPa for JFM season and at the surface for JAS season).

Vertical profiles of average temperature changes for JFM and JAS seasons are shown in Fig. 4. Given average global temperature change corresponds to the mean value of average changes at Northern and Southern Hemisphere. Simulated vertical profiles indicate that warming of the atmosphere is present at all considered levels for both hemispheres. It is notable that average hemispheric temperature change is larger for Northern than for Southern Hemisphere. An exception is the first level for boreal summer (JAS season), presumably due to influence of ice melting in the polar region and associated temperature decrease

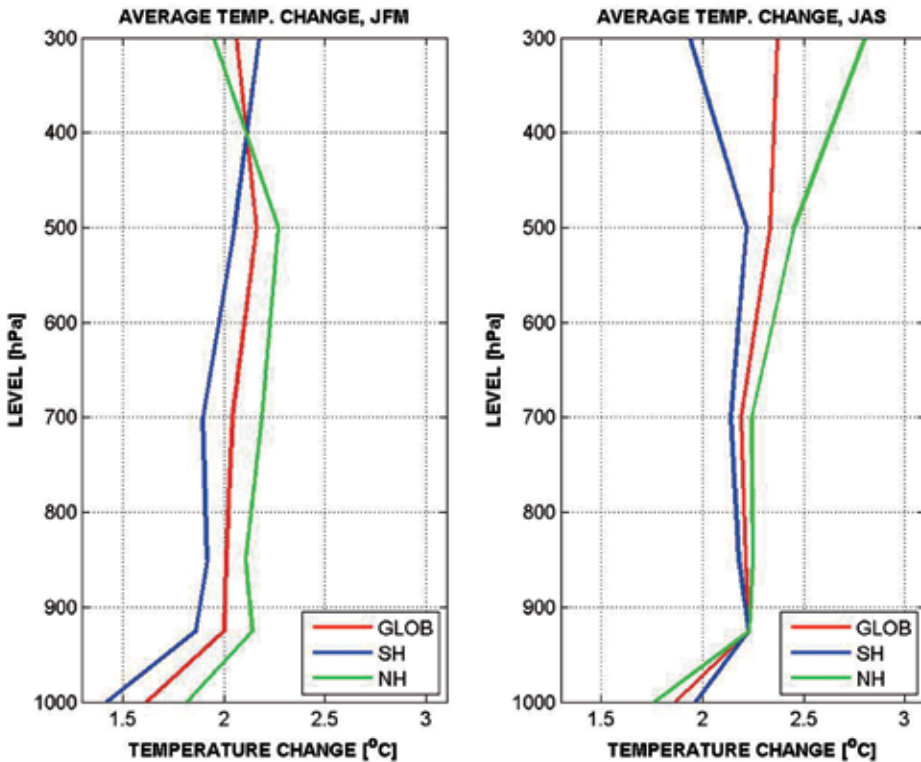


Figure 4. Average temperature change at selected vertical levels for JFM (left) and JAS (right) season.

as shown in Fig. 3a. During the southern summer (JFM), ice melting is not such extensive so neither the temperature decrease (Fig. 2a). Besides, the cooling is found over the polar region of Northern Hemisphere at 300 hPa during JFM season (Fig. 2d), but not over its southern counterpart during JAS season (Fig. 3d). Obviously, vertical structure of projected temperature change is seasonally depended. Both hemispheres as well as the whole globe experience an abrupt temperature increase between the surface and 925 hPa level (Fig. 4). Between 925 and 500 hPa, the air temperature increases at all considered levels keeping almost the same accretion. The shape of vertical profile is considerably changed above 500 hPa. Thus, the temperature increase is reduced on winter hemisphere and amplified on summer hemisphere (Fig. 4) resulting in the same hemispheric JFM temperature change at 400 hPa.

3.1.3. Direct and indirect effect of doubling CO_2 concentration

Besides atmospheric warming due to associated absorption and radiation processes, increased CO_2 concentration also indirectly affects lower boundary conditions causing SST increase and changes in sea-ice content. Here, we use targeted experiments (DIR and IND), to examine the direct and indirect effects of increased CO_2 concentration.

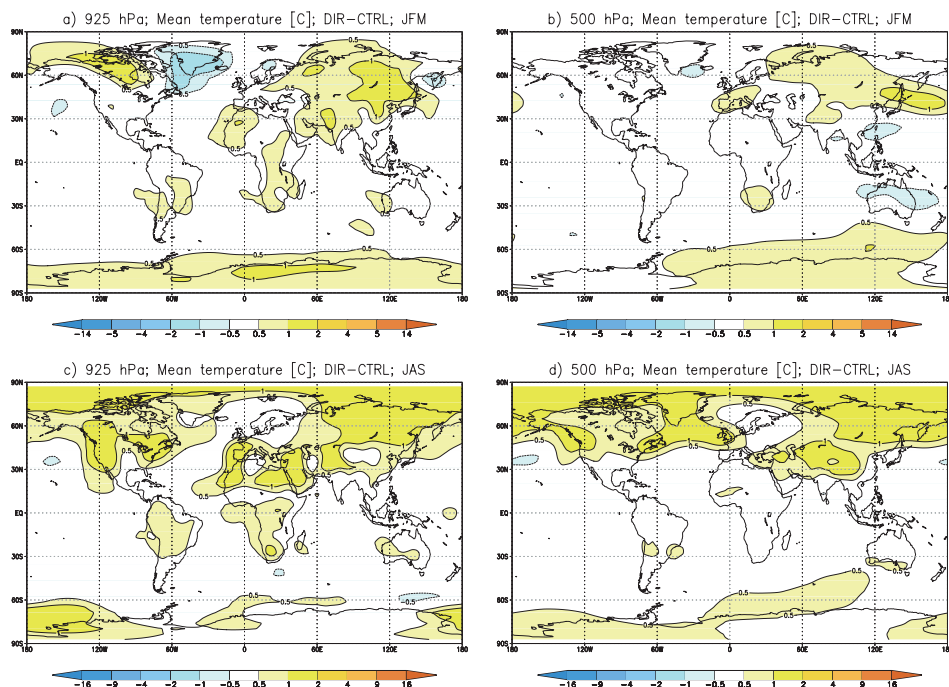


Figure 5. Differences between DIR and CTRL experiments in: (a) JFM season at 925 hPa; (b) JFM season at 500 hPa; (c) JAS season at 925 hPa; (d) JAS season at 500 hPa. Contours: 0.5, 1, 2, 4, 5, 14 °C in (a) and (b) and 0.5, 1, 2, 3, 4, 9, 16 °C in (c) and (d).

Figure 5 shows temperature difference between DIR and CTRL experiments for JFM and JAS seasons at 925 hPa and 500 hPa levels. Differences are mostly found over continental parts and are found to be much smaller in comparison with those from 2xCO₂ experiment (Figs. 2 and 3). For JFM season (Fig. 5a, b), differences in temperature over the Northern Hemisphere are positive over the continental part with negative local change occurring over Greenland. At 300 hPa level, changes are negative over the northern polar areas (not shown). During the JAS season (Figs. 5c, d), positive temperature changes occur over the polar areas of both hemispheres, with negative temperature change appearing at 300 hPa over the southern polar area (not shown).

Figure 6 represents changes between IND and CTRL experiments for JFM and JAS seasons at 925 hPa and 500 hPa. These changes are very similar to those between 2xCO₂ and CTRL (Fig. 2 and Fig. 3). Therefore, simulated temperature change shown in Figs. 2 and 3 may be predominantly attributed to the indirect effect of elevated CO₂ concentrations. This is in accordance with some earlier studies showing that indirect effect is much stronger than the direct (Hoering et al., 2008; Compo and Sardeshmukh, 2009; Deser and Phillips, 2009) and upholds the findings which indicate the change in lower boundary conditions as an important factor for climate change (e.g. Stephenson and Held, 1993; Hoerling et al., 2008; Compo and Sardeshmukh, 2009; Dommenges, 2009).

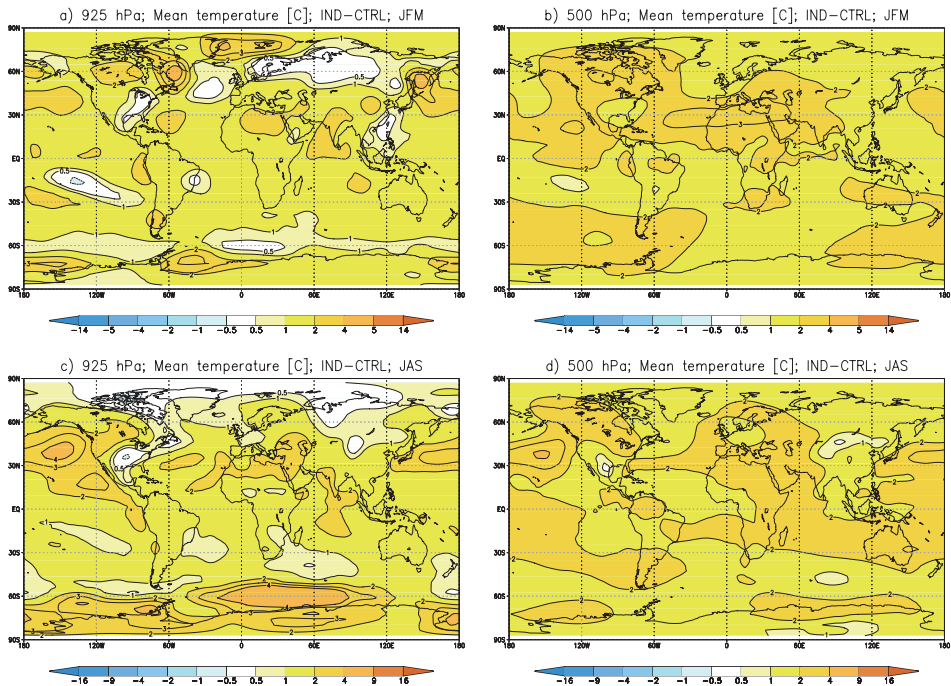


Figure 6. Same as Fig. 5, but for IND experiment.

The difference between direct and indirect effects is also noticeable in the meridional-vertical cross sections of zonal mean temperature, geopotential height and zonal wind (Fig. 7). Clearly, a tropospheric warming accompanied with stratospheric cooling is depicted in Fig. 7. However, while the tropospheric warming is associated with indirect effect (as shown in Fig. 7g), the cooling of the higher atmosphere is rather related to the direct CO_2 effects (Fig. 7d) and is stronger in polar areas. Relative contribution of direct and indirect CO_2 changes is also reflected in modification of atmospheric circulation. Thus, the difference between $2\times\text{CO}_2$ and CTRL experiment indicates positive geopotential anomalies in troposphere, while in the stratosphere there are negative anomalies (Fig. 7b). According to Figs. 7e and 7h, changes in the troposphere are provoked with indirect effects, while the stratospheric levels are affected with indirect CO_2 impact. Zonal wind response corresponds to the geopotential height showing the strengthening of the polar vortex at the winter hemisphere (Fig. 7c). Results for DIR and IND experiment reveal that the stronger polar vortex is result of direct CO_2 impact.

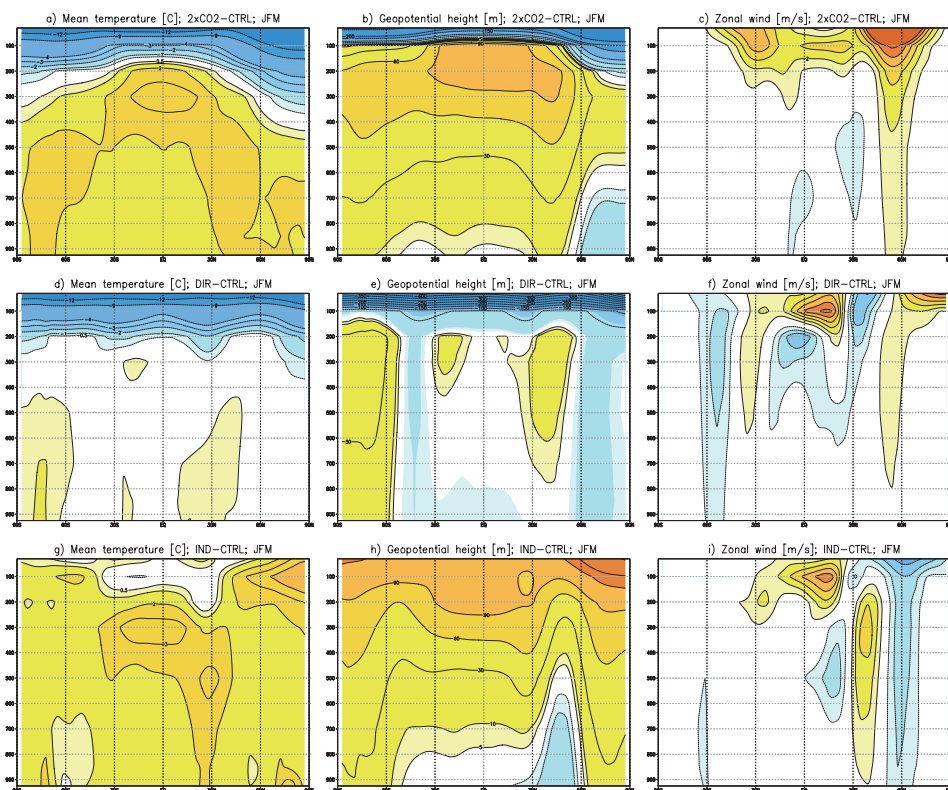


Figure 7. JFM vertical cross sections of changes in zonal mean temperature (left), geopotential height (middle) and zonal wind (right) for $2\times\text{CO}_2$ (top), DIR (middle) and IND (bottom) experiment comparing to CTRL experiment. Contours: 0.5, 1, 2, 3, 4, 9 and 12 °C in (a), (d) and (g); 5, 10, 30, 60, 90, 120 and 150 m in (b), (e), and (h); 5, 10, 30, 60, 90, 150, 200, 350 m in (c), (f) and (i)

3.2. Impact on zonal wind

Global zonal wind distributions for JFM and JAS seasons at 925 hPa and 500 hPa are shown in Fig. 8. Both of hemispheres are characterized with belts of positive values of u -wind presenting dominant westerly flow in the midlatitudes. In general, the flow is stronger on Southern Hemisphere and increases during the respective winter on the both hemispheres. Also, it strengthens with the height. Doubling of CO_2 concentration and associated changed lower boundary conditions modify zonal wind (Fig. 9). Here it is noteworthy to emphasize that proper interpretation of results requires consideration of sign of anomalies presented in Fig. 8 respecting the wind direction that prevails over considered region. Mostly, JFM zonal wind at 925 hPa is not changed considerably. Still, there is a belt of positive anomalies over the northern Atlantic and a part of European continent (Fig. 9a) indicating a strengthening of westerly flow that may possibly increase advection of the relatively warm and moist air from the Atlantic. Also, there is a considerable impact on zonal wind over the Pacific causing northward shift of westerly winds blowing over the northern Pacific. At higher levels, u -wind distribution is similar to that at 925 hPa, but with increased wind speeds (Figs. 8b, d). Doubled CO_2 concentration, together with associated modification of lower boundary conditions, considerably affects higher-level zonal winds (Figs. 9b, d). In general, changes in zonal wind are more pronounced during the winter of respective hemisphere.

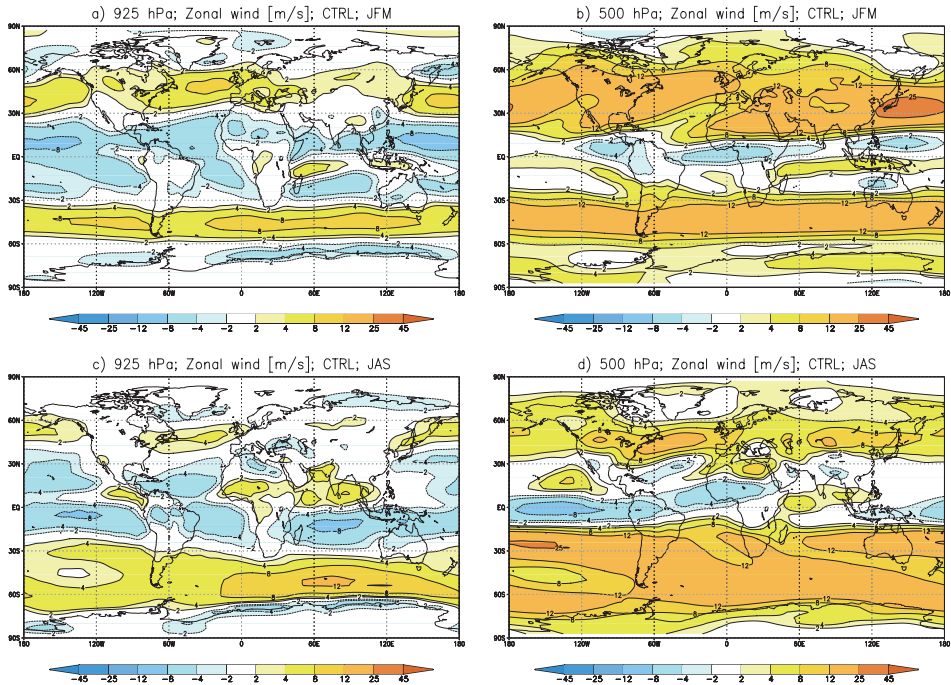


Figure 8. Zonal wind field in: (a) JFM season at 925 hPa; (b) JFM season at 500 hPa; (c) JAS season at 925 hPa; (d) JAS season at 500 hPa. Contours: 2, 4, 8, 12, 25 and 45 m/s.

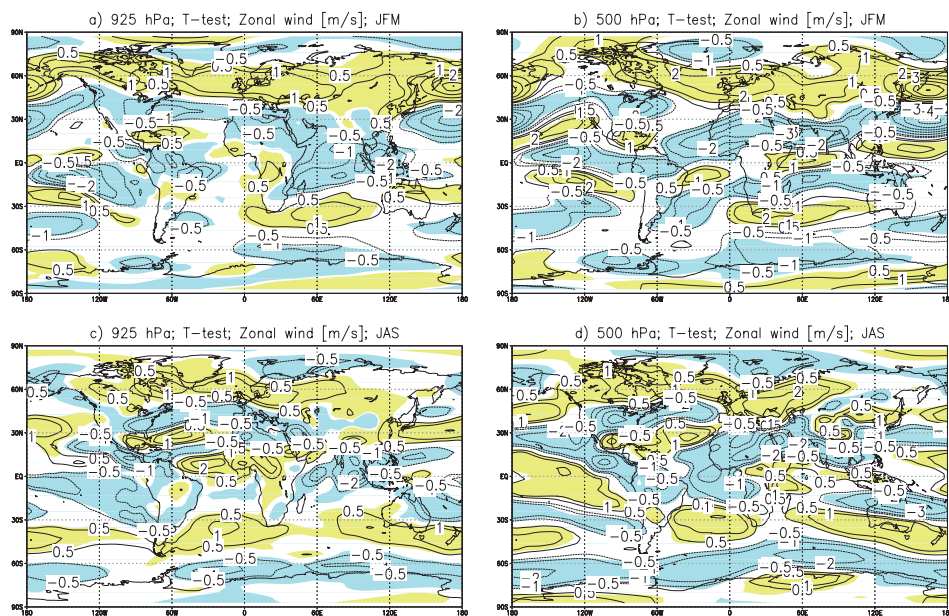


Figure 9. Zonal wind changes between 2xCO₂ and CTRL experiments in: (a) JFM season at 925 hPa; (b) JFM season at 500 hPa; (c) JAS season at 925 hPa; (d) JAS season at 500 hPa. Shaded areas are significant changes with positive changes marked as full lines and negative changes represented as dashed lines. Contours: 0.5, 1, 2, 3, 4, 5 and 6 m/s.

Maximal changes in zonal wind field are found at 300 hPa vertical level (not shown). Westerly winds are strengthened above north Atlantic and north Pacific at around 50°N, and over the southern part of world oceans at around 30° S. Changes in subtropical and polar jet streams are more pronounced and statistically significant for JFM season than for JAS. Therefore, simulated zonal wind changes indicate possible modification of jet streams in warmer climate conditions together with associated impact on weather, particularly during the winter.

3.3. Impact on precipitation

As a consequence of changes in temperature and wind in warmer climate conditions, modifying of precipitation is expected as well. Here, stratiform and convective precipitation simulated in 2xCO₂ experiment are compared with those obtained in CTRL.

3.3.1. Changes in stratiform precipitation

Differences between stratiform precipitation simulated in 2xCO₂ and CTRL experiments for JFM and JAS seasons are shown in Fig. 10. Increased precipitation in polar region and mid-latitudes with a few local extremes is found on the

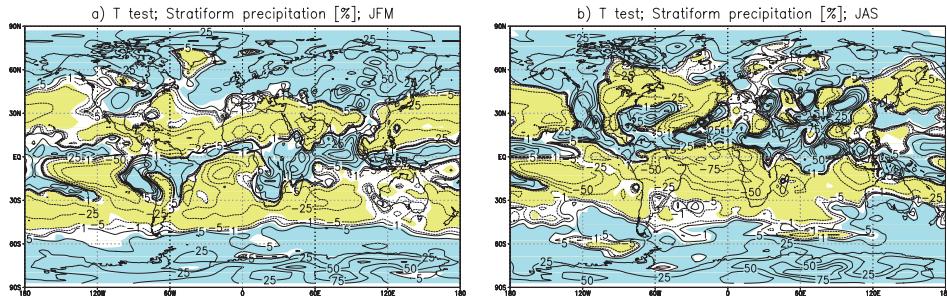


Figure 10. Stratiform precipitation changes between 2xCO₂ and CTRL experiment in (a) JFM season and (b) JAS season. Shaded areas are significant changes with positive changes marked as full lines and negative changes represented as dashed lines. Contours: 1, 5, 25, 50, 75 and 100%.

both hemispheres together with a belt of increased precipitation in equatorial region. For the winter (JFM) season, precipitation increase up to 0.4 mm/day occurs in a belt around 60° and southern of 60° S (Fig. 10a). On Northern Hemisphere, maximal precipitation differences occur over the north Pacific and Alaska, over the north Atlantic and sporadically over the Eurasian landmass. Increased precipitation over North America and Eurasian landmasses may be at least partially attributed to the wind changes. As depicted in Figs. 9.a and b, JFM zonal wind is increased over the north Atlantic and north Pacific. Consequently, the advection of warm moist air from the oceans is strengthened what increases precipitation over the land. During JAS season, positive differences with values up to 0.6 mm/day are extended along the coast of Antarctic, over Alaska and Greenland, while negative changes are found mainly above the oceans (Fig. 10). Precipitation gain of 4 mm/day is simulated over the western equatorial part of Africa, while maximal precipitation increase up to 5 mm/day is found over the Bangladesh indicating a possible strengthening of precipitation during the monsoon season.

In general, amplitude of stratiform precipitation change is larger for JAS (Fig. 10b) than for JFM (Fig. 10a) season. Still, area affected by precipitation change is broader for JFM than for JAS season. Precipitation changes also depict a seasonal dependence with increase in precipitation that is stronger during the winter, while a shrinking of area affected by increased precipitation is found during the summer season.

3.3.2. Changes in convective precipitation

Convective precipitation differences between 2xCO₂ and CTRL experiments for JFM and JAS seasons are shown in Fig. 11. It is notable that the largest changes occur in the area of intertropical convergence zone (ITCZ). For JFM season (Fig. 11a), the strongest precipitation increase is over the equatorial area.

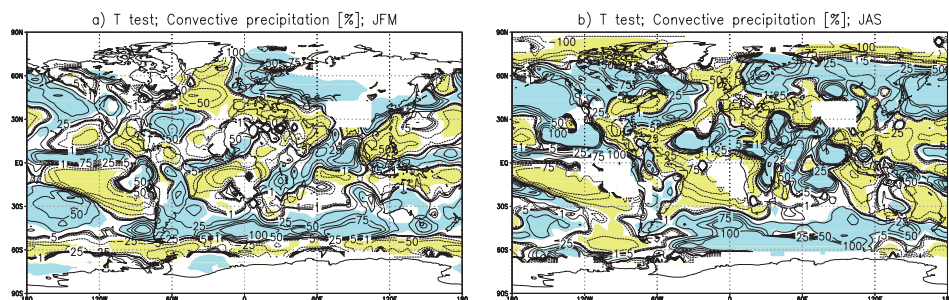


Figure 11. Same as Fig.10, but for convective precipitation.

Positive anomalies are simulated over the extratropical oceans of Southern Hemisphere, Australia and southern part of South America. The largest local decrease occurs over the tropical Pacific (around 140° W) reaching amount of 10 mm/day. For JAS season (Fig. 11b), the largest increase of 4 mm/day is depicted over the equatorial Africa, Indian Ocean and tropical Pacific. Slightly increased precipitation appears over the northern Pacific and part of western Atlantic (around 60° W), and in a belt around 60° N over the continental part of the Northern Hemisphere. The largest precipitation deficit occurs over the western Pacific and western equatorial Atlantic. For both seasons precipitation is increased over the western part of middle Atlantic (around 30° N). It is also notable that changes follow seasonal ITCZ shift (northward in JAS season).

Convective precipitation changes are in JAS season mostly significant over the continental part of northern hemisphere while in JFM season mostly over oceans (Fig. 11b). These results suggest that summer convective precipitation over the northern hemisphere is more sensitive to CO_2 doubling than winter precipitation. The cause of such difference in precipitation response, at least partially, is larger continental area at northern hemisphere that is warmed during the summer and thus supporting development of convection and convective precipitation. Contrary, stratiform precipitation does not show so pronounced difference between the hemispheres (Fig. 10).

In general, precipitation response to the doubled CO_2 shows substantial increase of winter precipitation in high latitudes (around 60° N and 60° S) which may be predominantly attributed to the increase of stratiform precipitation (cf. Figs. 10a and 11a). On the other hand, convective precipitation contributes to the increase of summer precipitation in the band around 60° N (particularly over the land; Fig. 11b). At the same time, precipitation is increased in the tropics, but decreased in the subtropics. This result is in accordance with the well known “wet get wetter, dry get drier” hypothesis (e.g. Held and Soden, 2006) which is also reflected in zonal mean of annual total precipitation (Fig. 12).

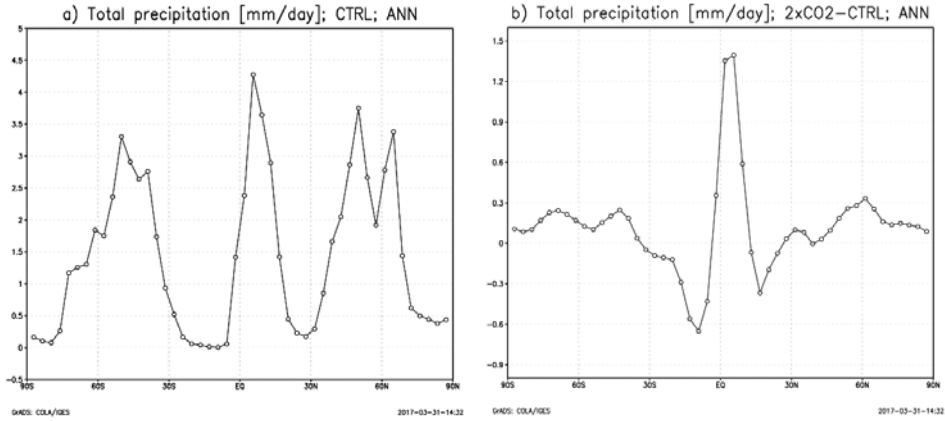


Figure 12. Zonal mean of annual: (a) total precipitation and (b) change 2xCO₂-CTRL.

4. Summary and conclusion

Changes in temperature, zonal wind and precipitation at selected vertical levels associated with doubling of CO₂ concentration, are analyzed by 35-member ensembles of 149-year long numerical integrations made with general circulation model ICTP AGCM. Such a large ensemble and very long integrations improves the statistical significance of the results. Here, we are focused on summer (JAS) and winter (JFM) seasons. Also, direct and indirect impact of increased CO₂ on temperature is compared utilizing two additional experiments (DIR and IND). Actual climate is presented by CTRL experiment which is forced with observed (monthly varying) SSTs, while for sea-ice and CO₂ concentration averaged values for 1961-1990 period are used. In warmer climate experiment (2xCO₂), doubled CO₂ concentration is simulated by setting the absorption radiation coefficient. In that experiment, interannual SST variability from CTRL experiment is superimposed to climatological SST and sea-ice obtained from coupled oceanic-atmospheric model realizations with doubled CO₂ concentration. Considering identical interannual SST variability in both experiments, mean field changes could be connected to climatological SST and sea-ice changes caused by increased CO₂ concentration.

Generally, ICTP AGCM simulations forced with doubled CO₂ concentrations result in a warming of Earth's surface and lower atmosphere accompanied with a stratospheric cooling. Certainly, since ICTP AGCM has only two layers as a crude representation of the stratosphere (*i.e.* the two top layers, 100 and 30 hPa), resolving of details regarding the stratospheric cooling cannot be expected, but it is in a qualitative agreement with some previous findings. Average warming at all selected levels for both seasons is around 2 °C. The largest local temperature changes occur at surface level in polar areas. Warming is larger at Northern Hemisphere, and is particularly pronounced over the continental parts.

Temperature increase of 2 °C for both seasons is found mostly over all continents, except South America and Africa. The largest average warming occurs at 500 hPa level in both seasons. Temperature changes at selected vertical levels are very similar, apart from 300 hPa level where temperature change has a zonal distribution with negative anomalies appearing over polar regions. However, at that level there is stratosphere, so negative anomalies indicate stratospheric cooling. Significant zonal wind changes occur mainly on Northern Hemisphere, while on Southern Hemisphere changes are significant at higher levels. Increase in CO₂ concentration causes changes in jet stream over Northern Hemisphere at all considered levels in both seasons, but with larger JFM amplitude. Significant jet stream changes over Southern Hemisphere occur at higher levels in JAS season. At lower levels in both seasons eastern wind over equatorial Pacific is increased, with larger changes in JFM season. Also changes are significant in both seasons over Europe and northern Africa. In JAS season eastern wind over tropical Atlantic is weakened, such as western wind at around 35° N. Changes over Atlantic are mostly significant in JAS season, while changes over northern Pacific in JFM season.

Stratiform precipitation is increased over polar areas and along the equator in both seasons, while precipitation deficit is simulated over oceans. Precipitation increase in mid-latitudes is larger at winter hemisphere and is relatively in accordance with zonal wind changes. In summer (JAS) season, significant stratiform precipitation changes occur over North America with increase over Florida and west coast, and decrease over the east coast. Over central Africa and central China stratiform precipitation is shifted eastward. At northern part of South America, significant precipitation decrease occurs in JAS season, while it is increased during JFM season. Also, in winter (JFM) season precipitation is significantly increased over the north Europe and Russia.

Largest convective precipitation increase occurs in the area of intertropical convergence zone and mid-latitudes of summer hemisphere. Convective precipitation changes are significant in JAS season above continental part of Northern Hemisphere as a result of larger land distribution that is heated in summer and that way supporting convection. Decrease in precipitation over southern part of tropical Pacific is also significant. Convective precipitation changes in JFM season over southern hemisphere are statistically not significant.

Overall, for both seasons the model produces enhanced precipitation in high latitudes (primary due to increased stratiform precipitation) and in the tropics (primary as a result of increased convective precipitation). In mid-latitudes of both hemispheres, the precipitation is enhanced mainly during respective winter. Simulated changes of total precipitation due to doubled CO₂ is in accordance with the well known “wet get wetter, dry get drier” hypothesis.

Increase of CO₂ concentration affects atmosphere in two ways: directly (by absorption and emission of long-wave radiation) and indirectly (due to changes in

lower boundary conditions that are consequence of increased CO₂). Difference in those two effects was estimated for temperature fields at 925 and 500 hPa. In troposphere, differences between DIR and CTRL experiments are much weaker and cover smaller area compared to those between 2xCO₂ and CTRL. On the other hand, differences between IND and CTRL are stronger and similar to the changes between 2xCO₂ and CTRL. These results suggest that indirect effect overcomes the direct one, and indicate that tropospheric change associated with doubled CO₂ is dominated by modification of lower boundary conditions (SST and sea-ice) rather than by absorption and radiation processes. On the other hand, modification of stratospheric temperature, geopotential height and zonal wind may be attributed to the direct CO₂ impact resulting in more intense polar vortex.

Acknowledgements – The work of Ivana Herceg-Bulić has been supported in part by Croatian Science Foundation under project 2831 (CARE).

References

- Bourke, W. (1974): A multilevel spectral model. I. Formulation and hemispheric integrations, *Mon. Wea. Rev.*, **102**, 687–701, DOI:10.1175/1520-0493(1974)102<0687:AMLSMI>2.0.CO;2.
- Bracco, A., Kucharski, F., Kallummal, R. and Molteni, F. (2004): Internal variability, external forcing and climate trends in multidecadal AGCM ensembles, *Clim. Dyn.*, **23**, 659–678, DOI:10.1007/s00382-004-0465-2.
- Compo, G. P. and Sardeshmukh, P. D. (2009): Oceanic influence on recent continental warming, *Clim. Dyn.*, **32**, 333–342, DOI:10.1007/s00382-008-0448-9.
- Deser, C. and Philips, A. S. (2009): Atmospheric circulation trends, 1950–2000: The relative roles of sea surface forcing and direct atmospheric radiative forcing, *J. Clim.*, **22**, 396–413, DOI:10.1175/2008JCLI2453.1.
- Dommenget, D. (2009): The ocean's role in continental climate variability and change, *J. Clim.*, **22**, 4939–4952, DOI:10.1175/2009JCLI2778.1.
- Gordon, C., Cooper, C., Senior, C. A., Banks, H. T., Gregory, J. M., Johns, T. C., Mitchell, J. F. B. and Wood, R. A. (2000): The stimulation of SST, sea ice extents and ocean heat transports in a version of the Hadley Centre coupled model without flux adjustments, *Clim. Dyn.*, **16**, 147–168, DOI:10.1007/s003820050010.
- Gregory, J. M., Stott, P. A., Cresswell, D. J., Rayner, N. A., Gordon, C. and Sexton, D. M. H. (2002): Recent and future changes in Arctic sea ice simulated by the HadCM3 AOGCM, *Geophys. Res. Lett.*, **29**(24), 28–1–28–4, DOI:10.1029/2001GL014575.
- Hannachi, A. and Turner, A. G. (2008): Preferred structures in large-scale circulation and the effect of doubling greenhouse gas concentration in HadCM3, *Q. J. R. Meteorol. Soc.*, **134**, 469–480, DOI:10.1002/qj.236.
- Held, I. M. and Soden, B. J. (2006): Robust responses of the hydrological cycle to global warming, *J. Clim.*, **19**, 5686–5699, DOI:10.1175/JCLI3990.1.

- Held, I. M. and Suarez, M. J. (1994): A proposal for the intercomparison of dynamical cores of atmospheric general circulation models, *Bull. Amer. Meteor. Soc.*, **75**, 1825–1830, DOI:10.1175/1520-0477(1994)075<1825:APFTIO>2.0.CO;2
- Henderson-Sellers, B. (1987): Modelling sea surface temperature rise resulting from increasing atmospheric carbon dioxide concentrations, *Clim. Change*, **11**, 349–359, DOI:10.1007/BF00143324.
- Herceg-Bulić, I. (2010): The sensitivity of climate response to the wintertime Nino3.4 sea surface temperature anomalies of 1855–2002, *Int. J. Climatol.*, **32**, 22–32, DOI:10.1002/joc.2255.
- Herceg-Bulić, I. and Branković, Č. (2006): Seasonal climate sensitivity to the sea-ice cover in an intermediate complexity AGCM, *Geofizika*, **23**, 37–58.
- Herceg-Bulić, I., Branković, Č. and Kucharski, F. (2012): Winter ENSO teleconnections in a warmer climate, *Clim. Dyn.*, **38**, 1583–1613, DOI:10.1007/s00382-010-0987-8.
- Hirota, T., Pomeroy, J. W., Granger, R. J. and Maule, C. P. (2002): An extension of the force-restore method to estimating soil temperature at depth and evaluation for frozen soils under snow, *J. Geophys. Res.*, **107**(D24), ACL 11-1–ACL 11-10, DOI:10.1029/2001JD001280.
- Hoerling, M., Kumar, A., Eischeid, J. and Jha, B. (2008): What is causing the variability in global land temperature?, *Geophys. Res. Lett.*, **35**, L23712, DOI:10.1029/2008GL035984.
- IPCC (2007): *Climate change 2007: The Physical Science Basis. Contribution of working group I to the Fourth Assessment Report of the Intergovernmental Panel on Climate Change*, edited by Solomon, S., Quin, D., Manning, M., Chen, Z., Marquis, M., Averyt, K. B., Tignor, M. and Miller, H. L. Cambridge University Press, Cambridge, United Kingdom and New York, NY, USA.
- IPCC (2014): *Climate Change 2014: Synthesis Report. Contribution of Working Groups I, II and III to the Fifth Assessment Report of the Intergovernmental Panel on Climate Change*, edited by Core Writing Team, Pachauri, R. K. and Meyer, L. A. IPCC, Geneva, Switzerland, 151 pp.
- Jin, Z., Stamnes, K., Weeks, W. F. and Tsay, S. C. (1994): The effect of sea ice on the solar energy budget in the atmosphere-sea ice-ocean system: A model study, *J. Geophys. Res.*, **99**, 25281–25294, DOI:10.1029/94JC02426.
- Kalnay, E., Kanamitsu, M., Kistler, R., Collins, W., Deaven, D., Gandin, L., Iredell, M., Saha, S., White, G., Woollen, J., Zhu, Y., Leetmaa, A., Reynolds, R., Chelliah, M., Ebisuzaki, W., Higgins, W., Janowiak, J., Mo, K. C., Ropelewski, C., Wang, J., Jenne, R. and Joseph, D. (1996): The NCEP/NCAR 40-year reanalysis project, *Bull. Amer. Meteor. Soc.*, **77**, 437–471, DOI:10.1175/1520-0477(1996)077<0437:TNYRP>2.0.CO;2.
- Kucharski, F., Molteni, F., King, M. P., Farneti, R., Kang, I.-S. and Feudale, L. (2013): On the need of intermediate complexity general circulation models: A “SPEEDY” example, *Bull. Amer. Meteor. Soc.*, **94**, 25–30, DOI:10.1175/BAMS-D-11-00238.1.
- Manabe, S., Bryan, K. and Spelman, M. (1990): Transient response of a global ocean-atmosphere model to a doubling of atmospheric carbon dioxide, *J. Phys. Oceanogr.*, **20**, 722–749, DOI:10.1175/1520-0485(1990)020<0722:TROAGO>2.0.CO;2.
- Manabe, S., Stouffer, R., Spelman, M. and Bryan, K. (1991): Transient responses of a coupled ocean-atmosphere model to gradual changes of atmospheric CO₂. Part I. Annual mean response, *J. Clim.*, **4**, 785–818, DOI:10.1175/1520-0442(1991)004<0785:TROACO>2.0.CO;2.
- Meehl, G. A. and Washington, W. M. (1996): El Niño-like climate change in a model with increased atmospheric CO₂ concentrations, *Nature*, **382**, 56–60, DOI:10.1038/382056a0.
- Meehl, G. A., Teng, H. and Branstator, G. (2006): Future changes of El Niño in two global coupled climate model, *Clim. Dyn.*, **26**, 549–566, DOI:10.1007/s00382-005-0098-0.

- Meehl G.A., Stocker, T. F., Collins, W. D., Friedlingstein, P., Gaye, A. T., Gregory, J. M., Kitoh, A., Knutti, R., Murphy, J. M., Noda, A., Raper, S. C. B., Watterson, I. G., Weaver, A. J. and Zhao, Z. C. (2007): Global climate projections, in: *Climate Change 2007: The Physical Science Basis. Contribution of Working Group I to the Fourth Assessment Report of the Intergovernmental Panel on Climate Change*, edited by Solomon, S., Qin, D., Manning, M., Chen, Z., Marquis, M., Averyt, K. B., Tignor, M. and Miller, H. L. Cambridge University Press, Cambridge, 744–845.
- Merryfield, W. J. (2006): Changes to ENSO under CO₂ doubling in multimodel ensemble, *J. Clim.*, **19**, 4009–4027, DOI:10.1175/JCLI3834.1.
- Molteni, F. (2003): Atmospheric simulations using GCM with simplified physical parametrizations. I: Model climatology and variability in multi-decadal experiments, *Clim. Dyn.*, **20**, 175–191, DOI:10.1007/s00382-002-0268-2.
- Pope, V., Gallani, M. L., Rowntree, P. R., Stratton, R. A. (2000): The impact of new physical parametrizations in the Hadley Centre climate model: HadAM3, *Clim. Dyn.*, **16**, 123–146, DOI:10.1007/s003820050009.
- Rayner, N. A., Parker, D. E., Horton, E. B., Folland, C. K., Alexander, L. V., Rowell, D. P., Kent, E. C. and Kaplan, A. (2003): Global analyses of sea surface temperature, sea ice, and night marine air temperature since the late nineteenth century, *J. Geophys. Res.*, **108**, 4407, DOI:10.1029/2002JD002670.
- Shindell, D. T., Miller, R. L., Schmidt, G. A. and Pandolfo, L. (1999): Simulation of recent northern winter climate trends by greenhouse-gas forcing, *Nature*, **399**, 452–455, DOI:10.1038/20905.
- Smith, T. M. and Reynolds, R. W. (2004): Improved extended reconstruction of SST (1855–1997), *J. Clim.*, **6**, 1859–1870, DOI:10.1175/1520-0442(2004)017<2466:IEROS>2.0.CO;2.
- Solomon, S., Plattner, G.-K., Knutti, R. and Friedlingstein, P. (2009): Irreversible climate change due to carbon dioxide emissions, *Proceedings of the National Academy of Sciences*, **106**, 1704–1709.
- Stephenson, D. B. and Held, I. M. (1993): GCM response of northern winter stationary waves and storm tracks to increasing amounts of carbon dioxide, *J. Clim.*, **6**, 1859–1870, DOI:10.1175/1520-0442(1993)006<1859:GRONWS>2.0.CO;2.
- Thompson, D.W.J., Seidel, D. J., Randel, W. J., Zou, C.-Z., Butler, A. H., Mears, C., Osso, A., Long, C. and Lin, R., (2012): The mystery of recent stratospheric temperature trends, *Nature*, **491**, 692–697, DOI:10.1038/nature11579.
- Turner, A. G., Inness, P. M. and Slingo, J. M. (2007): The effect of doubled CO₂ and model basic state biases on the monsoon ENSO system. I: Mean response and interannual variability, *Quart. J. Roy. Meteor. Soc.*, **133**, 1143–1157, DOI:10.1002/qj.82.
- Washington, W. M. and Meehl, G. A. (1989): Climate sensitivity due to increased CO₂: Experiments with a coupled atmosphere and ocean general circulation model, *Clim. Dyn.*, **4**, 1–38, DOI:10.1007/BF00207397.
- Wilks, D. S. (2006): Statistical methods in the atmospheric sciences, *Inter. Geophys.*, **91**, 140–141.

SAŽETAK

Simulacije klimatskog odziva na udvostručene koncentracije ugljičnog dioksida u atmosferi korištenjem jednostavnog modela opće cirkulacije atmosfere*Irena Nimac i Ivana Herceg-Bulić*

Atmosferski odziv na udvostručene koncentracije ugljičnog dioksida istražen je pomoću 35-članog ansambla kreiranog relativno jednostavnim modelom opće cirkulacije atmosfere. Promjene srednjih stanja analizirane su za zimsku (siječanj-veljača-ožujak) i ljetnu (srpanj-kolovoz-rujan) sezonu. Rezultati pokazuju da udvostručenje koncentracije CO₂ uzrokuje zatopljenje od oko 2 °C na svim promatranim nivoima. U prizemnom sloju do najvećih promjena dolazi u polarnim područjima, dok u višim slojevima veće zatopljenje zahvaća uglavnom kontinentalne dijelove Sjeverne hemisfere. Porast temperature na 300 hPa popraćen je zahlađenjem nad polarnim područjima. Na nivoima iznad 300 hPa dolazi do globalnog pada temperature. Signifikantne promjene mlazne struje javljaju se na Sjevernoj hemisferi te su izraženije u zimu. Do značajnog porasta stratiformne oborine dolazi na zimskoj hemisferi u višim geografskim širinama, dok se smanjenje javlja uglavnom iznad oceana. Signifikantan porast konvektivne oborine javlja se ljeti iznad kontinenta Sjeverne hemisfere. U južnom dijelu tropskog Pacifika u obje sezone dolazi do smanjenja stratiformne i konvektivne oborine. Također je pokazano da neizravni utjecaj porasta koncentracija CO₂, tj. promjene donjih graničnih uvjeta koje su posljedica porasta CO₂ imaju veći doprinos zatopljenju troposfere od izravnog utjecaja koji se odvija putem apsorpcijsko-radijacijskih procesa na samim molekulama CO₂.

Ključne riječi: klimatske promjene, udvostručena koncentracija CO₂, model SPEEDY, izravan utjecaj, neizravan utjecaj

Corresponding author's address: Irena Nimac, Meteorological and Hydrological Service of Croatia, Grič 3, HR-10 000 Zagreb, Croatia; tel: +385 1 460 5932; e-mail: irena.nimac@gmail.com

